JACS
JOURNAL OF THE AMERICAN CHEMICAL SOCIETY
Communication
pubs.acs.org/JACS

Flow-Assisted 2D Polymorph Selection: Stabilizing Metastable Monolayers at the Liquid–Solid Interface

Shern-Long Lee,[†] Zhongyi Yuan,[‡] Long Chen,[‡] Kunal S. Mali,*[,†] Klaus Müllen,*[,‡] and Steven De Feyter*[,†]

[†]KU Leuven-University of Leuven, Department of Chemistry, Division of Molecular Imaging and Photonics, Celestijnenlaan 200F, B-3001 Leuven, Belgium

[‡]Max Planck Institute for Polymer Research, D-55128 Mainz, Germany

Supporting Information

ABSTRACT: Controlling crystal polymorphism constitutes a formidable challenge in contemporary chemistry. Two-dimensional (2D) crystals often provide model systems to decipher the complications in 3D crystals. In this contribution, we explore a unique way of governing 2D polymorphism at the organic liquid–solid interface. We demonstrate that a directional solvent flow could be used to stabilize crystalline monolayers of a metastable polymorph. Furthermore, flow fields active within the applied flow generate millimeter-sized domains of either polymorph in a controlled and reproducible fashion.

Polymorphism is a highly emergent property by virtue of which molecules are able to crystallize in more than one type of nearly isoenergetic packing in the solid state.[1] Besides the heightened commercial interest due to the discovery of multiple crystal forms of drug molecules, the research on polymorphism is important for resolving a number of fundamental issues relevant to crystallization itself.[2] This phenomenon, however, is not limited to bulk crystallizations and has been observed abundantly during two-dimensional (2D) crystallization of organic molecules at the organic liquid–solid interface.[3−5] Such 2D crystals often serve as excellent model systems for 3D crystals. Thus, understanding 2D crystal polymorphism constitutes an important step toward comprehension and control of crystal polymorphism in general.

Studying 2D polymorphism at the liquid–solid interface using scanning tunneling microscopy (STM)[6] is a relatively simple and efficient approach as the evolution of different crystal (pseudo)polymorphs can be monitored, sometimes in a time dependent[7−9] fashion, unravelling the kinetics and thermodynamics of their formation at the molecular level. Apart from the typical factors such as temperature[10−12] and solvent,[13,14] which are also known to influence bulk crystal polymorphism, the unique nature of this interface allows observation of concentration dependent polymorphism,[9,15,16] a phenomenon rather alien to bulk crystallizations. Similar to 3D crystallizations, metastable polymorphs[7,9] are often observed at the liquid–solid interface. Understanding the formation of such metastable polymorphs and their evolution to stable polymorphs holds a key to uncovering the hidden mysteries of crystallization processes in general. However, such metastable polymorphs are often short-lived, and their isolation is a major challenge in crystal structure studies.

In this contribution, we demonstrate the use of a directional solvent flow[17] to select one crystalline polymorph over the other at the liquid–solid interface. Importantly, we show that the flow-assisted polymorph selection allows stabilization of a polymorph that is otherwise metastable at room temperature (24–26 °C). In our simple approach, a capillary force is generated by contacting a clean tissue paper to the substrate immediately after drop casting a 1,2,4-trichlorobenzene (TCB) solution of quaterrylene diimide[18] (QDI, Scheme 1a) on the highly oriented pyrolytic graphite (HOPG) surface. Depending on the direction with respect to the substrate lattice it is applied, the flow generates a particular crystalline polymorph in a controlled and reproducible fashion (Scheme 1b). Moreover, flow fields operating within the nanoscale confinement of the liquid–solid interface force the molecular assembly into

Scheme 1. (a) Molecular Structure of QDI; (b) Schematic of the Flow-Assisted Polymorph Selection Process[a]

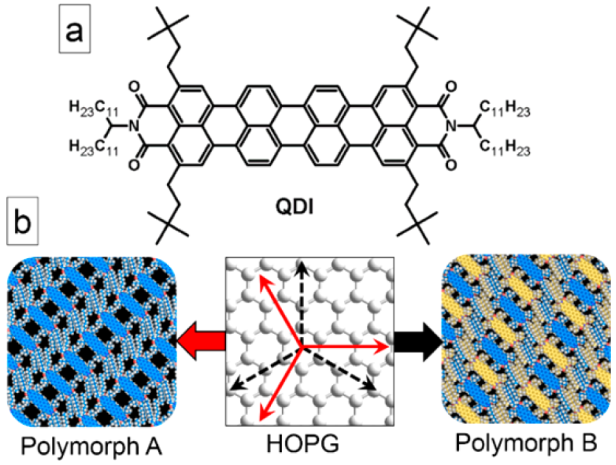

[a]Depending on whether the flow is applied along the main symmetry axes (red arrows on HOPG lattice) or along the normals to the main axes (black dashed arrows) polymorph A or polymorph B is selected at the liquid–solid interface, respectively.

Received: April 7, 2014
Published: May 14, 2014

dx.doi.org/10.1021/ja503466p | J. Am. Chem. Soc. 2014, 136, 7595−7598

supersized (millimeter^2) domains, which are otherwise not formed upon dropcasting.

QDI is a member of the rylene family of organic dyes and consists of four naphthalene units fused via their *peri* positions. Compared to lower rylene derivatives, QDIs have near-infrared (NIR) absorbing characteristics with high extinction coefficients making them suitable for use in a wide range of applications in optoelectronic devices such as solar cells, NIR photodetectors, and light-emitting diodes.[19] The rigid polycyclic aromatic backbone with a relatively high aspect ratio (4.4) imparts an anisotropic, ribbon-like shape to the QDI molecule. This structural feature makes QDI an ideal candidate for flow treatment, a process that has been used extensively in the past to align various 1D nanostructures.[20] In fact, while investigating the effect of flow treatment on the assembly behavior we fortuitously came across the dimorphic 2D crystallization behavior of QDI.

Figure 1a displays an STM image depicting the coexistence of two nearly identical polymorphs of QDI obtained upon dropcasting a TCB solution onto a freshly cleaved HOPG surface. Both of the polymorphs consist of linear rows of molecules. A characteristic feature of polymorph *B* is the STM contrast variation within molecular rows. Every alternate molecule in a row of polymorph *B* appears bright (dark). This contrast variation possibly arises due to the incommensurate registry of every other QDI aromatic core with the HOPG lattice. A close inspection of the STM image shows the disparity in the packing density of molecules in the two polymorphs. Small-scale STM images provided in Figure 1b and 1c together with corresponding molecular models (Figure 1d and 1e) further highlight the structural aspects of molecular packing. Although both polymorphs consist of rows of molecules, the packing density in polymorph *A* (1 molecule/unit cell, 0.16 molecule/nm^2) is lower than that in *B* (2 molecules/unit cell, 0.21 molecule/nm^2). Another striking difference is the orientation of the row axis with respect to the main symmetry axis of the HOPG for the two polymorphs. The molecular rows are oriented along one of the main symmetry axes of the HOPG lattice for polymorph *A* whereas they run nearly (±8°) along the normal to the main symmetry axis of HOPG for *B*.

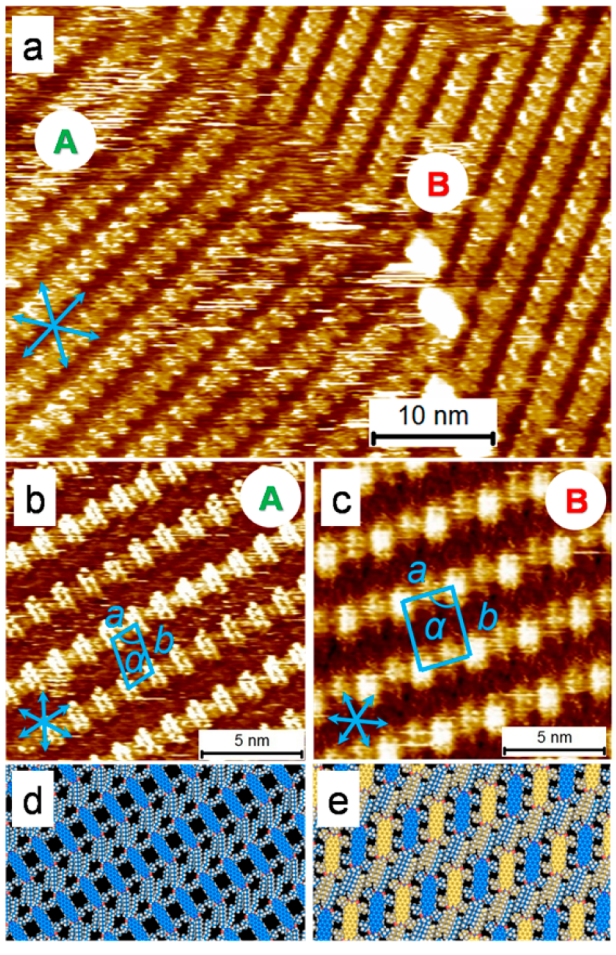

Figure 1. 2D crystal polymorphism of QDI. (a) STM image depicting the coexistence of the two polymorphs *A* and *B* at the TCB/HOPG interface (C_{QDI} = 1.2 × 10^{-5} M). The graphite symmetry axes are shown in the lower left corner of each image. (b, c) Small scale STM images showing molecular packing in polymorph *A* and *B*. The unit cell parameters: (for *A*) a = 1.70 ± 0.14 nm, b = 3.71 ± 0.16 nm, α = 83.4 ± 1.2°; (for *B*) a = 2.77 ± 0.15 nm, b = 3.52 ± 0.18 nm, α = 87.3 ± 1.1°. (d, e) Molecular models for polymorph *A* and *B*, respectively. Imaging conditions: (for (a)) V_{bias} = 700 mV, I_{set} = 60 pA; (for (b, c)) V_{bias} = 600 mV, I_{set} = 100 pA.

Apart from the differences in their 2D crystal structures, there are significant differences in the domain size, surface coverage, and stability of the two polymorphs. Polymorph *A* is the major phase (~85%) on the HOPG surface with large domains (>200 × 200 nm^2) whereas polymorph B is the minor phase (~15%) with relatively smaller domains that often exist near graphite step-edges. Polymorph *B* is typically observed within a few minutes after deposition upon which it is gradually replaced by polymorph *A*. This transition can be followed by STM in a time-dependent fashion (Figure S1 in the Supporting Information (SI)). At longer times (~3 h) after deposition, only polymorph *A* exists on the surface indicating its higher thermodynamic stability with respect to *B*. An intriguing aspect concerning the relative stability of the two polymorphs is that, despite being the high-density phase, polymorph *B* was always found to be metastable under diverse experimental conditions. The surface coverage of polymorph *B* did not change significantly upon varying the solution concentration thus ruling out a case of concentration dependent polymorphism[15] (Figure S2).

In order to further confirm the relative stabilities of the two polymorphs, we attempted to influence the 2D crystallization process by varying the deposition temperature. It must be noted that the STM measurements were carried out at room temperature. Upon deposition onto the HOPG substrate held at 70 °C, polymorph *A* is formed exclusively and remains stable for several hours, providing additional evidence for its higher thermodynamic stability (Figures S3−S4). Concurrently, ensuring that the nucleation occurs rapidly by lowering the substrate temperature to 5 °C, polymorph *B* could be obtained almost exclusively (Figures S5−S6). The crystallites of polymorph *B*, however, are gradually transformed into those of polymorph *A* within 1 h after deposition. These experiments indicate that polymorph *B* is the kinetic form of the 2D crystal.[7] Such a structural transition is widely observed in 3D crystallizations and is known as the Ostwald's rule of stages.[21] This rule describes that crystal formation often occurs through a series of intermediate metastable phases prior to formation of the thermodynamically stable structure. The general applicability of this rule has not been verified for 2D crystallizations; however, recent studies reveal that the 2D patterns obtained at

dx.doi.org/10.1021/ja503466p | J. Am. Chem. Soc. 2014, 136, 7595−7598

the liquid−solid interface are often kinetically trapped structures with high barriers for desorption.[4,22]

Since polymorph *B* is metastable under normal experimental conditions, any manipulation under thermodynamic control is born to be unsuccessful. Bearing this in mind, we attempted stabilization of polymorph *B* using a somewhat unconventional stimulus. In the following, we illustrate how a capillary force generated by the flow of a solvent in a highly confined space offered by the liquid−solid interface can influence the selection of a polymorph. Although relatively nascent, the concept of directional flow has been exploited to align 2D molecular nanostructures with large uniaxially aligned domains of organic molecules.[17] We recently demonstrated that the flow induced alignment strategy is not limited to monolayers and could be efficiently used to fabricate large area well-aligned multilayered thin films. The general consensus that has emerged from these studies is that the success of the flow alignment process depends critically on the specific directions along which the flow is applied.[23] We reasoned that the propensity of the two polymorphs to crystallize along different symmetry directions of HOPG will allow us to control the expression of each polymorph provided that the shear flow is applied along appropriate directions.

To test the feasibility of flow-assisted polymorph selection, a 10 μL droplet of QDI solution in TCB was applied onto the HOPG substrate and the solution was immediately contacted by Kimwipe tissue paper such that the flow was generated along one of the main symmetry axes of the HOPG lattice. STM imaging of the surface revealed that the flow creates large domains of polymorph *A* (Figure 2a, c) extending over 4 × 4 mm^2 (Figure S7). This observation is in line with previous studies which revealed that a directional flow can create supersized molecular domains thus reducing the polycrystallinity of the thin film.[17,23] The efficiency of the flow induced alignment diminishes ∼4 mm away from the contact line which means that smaller crystallites could be found in these regions.

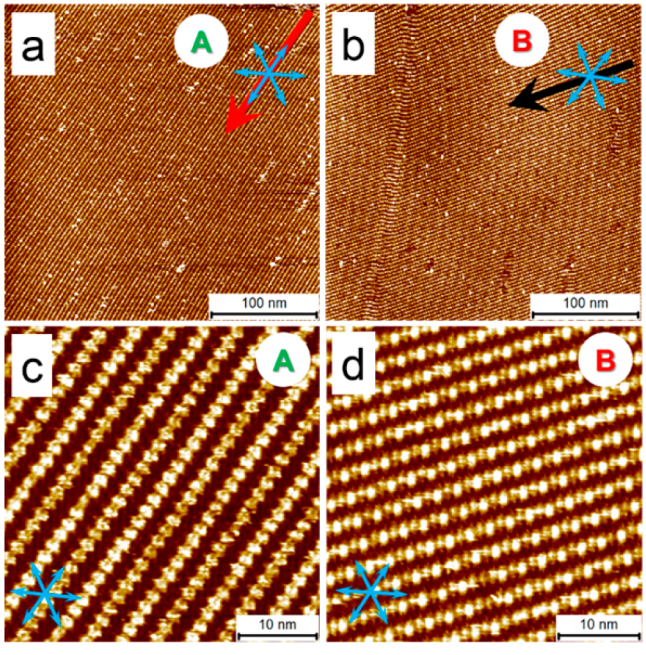

Figure 2. Flow-assisted 2D polymorph selection. (a, b) Large scale STM images showing the flow-assisted stabilization of polymorph *A* and, polymorph *B* into large domains, respectively. The flow was applied along the main symmetry axes of HOPG (red arrow) for obtaining polymorph *A* and along the normal to the main symmetry axis (black arrow) for stabilizing large networks of polymorph *B*. Small scale STM images provided in (c, d) confirm the formation of each polymorph. Imaging conditions: V_{bias} = 750 mV, I_{set} = 100 pA.

Application of flow along the normal to one of the main symmetry axes of the HOPG lattice also leads to the formation of large domains; however, STM imaging at smaller scales discloses that the 2D crystal now consists of polymorph *B* (Figure 2b, d). 2D crystallites of polymorph *B* obtained in this fashion also extend over 4 × 4 mm^2 and remain stable under ambient conditions for up to 6 h (Figure S7). The region out of the active 4 × 4 mm^2 zone consisted of smaller crystallites of polymorph *A*. This observation demonstrates that, under the influence of a directional flow, the metastable polymorph *B* (1) can be nucleated and further grown with significant surface coverage and (2) once formed it remains stable on the surface for several hours. These results essentially illustrate that, by modifying the conditions during 2D crystallization via application of a confined and directional flow, it is possible to select one of the two polymorphs.[24]

In order to understand the role of shear flow in stabilizing the two polymorphs, one needs to work out the factors that contribute to their intrinsic stability. The metastability of polymorph B at room temperature possibly arises due to (1) steric repulsions between 3,3-dimethyl-1-butyl side chains attached to the aromatic residues of the QDI molecules and (2) the overcrowding of the alkyl chains in between molecular rows thus forcing some alkyl chains to back-fold in the supernatant liquid phase (also note that the unit cell vector b of polymorph B is smaller than that of polymorph A). Low temperature deposition experiments indicated that polymorph *B* nucleates faster than polymorph *A*. The reduced nucleation barrier for polymorph *B* could be a result of higher enthalpic interactions due to close packing. The less dense polymorph *A*, on the other hand, could be stabilized by coadsorption of solvent molecules in the monolayer. STM images together with molecular models provided in Figure S8 in the SI indicate the presence of small packets within the monolayer of polymorph *A*, which could act as sites for solvent cocrystallization. Solvent stabilization of such relatively less dense polymorphs is well reported in the literature.[4,12]

Given that polymorph *B* has a lower barrier for nucleation, it is readily expected that the application of flow modifies the 2D crystallization process at the level of nucleation. This hypothesis is further supported by experimental evidence where it was found that the flow process only works when it is applied immediately (within a few seconds) after the deposition of the solution droplet. Polymorph *B* could not be amplified when the flow was applied well after the deposition of the solution droplet. This indicates that once polymorph *A* is formed on the surface, it remains stable even under the influence of flow.

Basically, the flow produces an environment that is conducive for kinetic stabilization of polymorph *B*. This in turn relates to significantly increased transport processes under the influence of flow in contrast to 2D crystallization upon simple dropcasting. It can be readily envisaged that the deposition of molecules from the solution phase to the self-assembled phase would be greatly enhanced under such a dynamic environment once the flow direction selects which polymorph nucleates onto the surface. The subtle yet important molecule−substrate interactions[25] together with the propensity of the two

dx.doi.org/10.1021/ja503466p | J. Am. Chem. Soc. 2014, 136, 7595−7598

polymorphs to crystallize along different symmetry axes of the substrate lattice thus allows precise control over the nucleation and growth of each polymorph. Similar processes have often been used for enhanced crystallization of semicrystalline polymers under the influence of shear flow.[26]

Due to its metastable nature at room temperature, polymorph *B* could be converted back to polymorph *A* by simply adding a drop of neat TCB onto the flow processed sample. A sequence of STM images provided in Figure S9 of the SI shows the time dependent transition of polymorph *B* into polymorph *A*. Such a transition is possibly driven by increased adsorption−desorption dynamics initiated by the added solvent, which was otherwise reduced in the almost dry monolayer obtained after the flow treatment. Polymorph *A* obtained in this fashion never furnished polymorph *B* even upon drying the sample, further eliminating the possibility of concentration controlled polymorphism.

In essence, we have used a kinetic flow process to influence 2D polymorph selection at the liquid−solid interface. While solvent flow has often been employed to align 1D nanostructures and for enhanced nucleation of semicrystalline polymers, this is the first instance of its use to influence the nucleation and growth of 2D polymorphs of small organic molecules. The unique nature of the liquid−solid interface coupled with specific epitaxial stabilization of each polymorph on HOPG allowed us to apply this nonequilibrium process to select a given polymorph in a controlled manner. Since metastable polymorphs are often short-lived species, the solution flow approach, which allows one to study their formation and structure, will contribute significantly to our understanding of crystallization processes in general. From the applied perspective, such large area thin films of metastable polymorphs could be used to seed the growth of the same metastable polymorph in 3D thus extending the applicability of this approach to bulk crystallizations. Finally, the flow-assisted thin film formation could also be beneficial for fabrication of large area oriented films of functional molecules typically used in organic thin film transistors.

■ ASSOCIATED CONTENT

Supporting Information

Experimental methods and additional STM data. This material is available free of charge via the Internet at http://pubs.acs.org.

■ AUTHOR INFORMATION

Corresponding Authors

Kunal.Mali@chem.kuleuven.be
muellen@mpip-mainz.mpg.de
Steven.DeFeyter@chem.kuleuven.be

Notes

The authors declare no competing financial interest.

■ ACKNOWLEDGMENTS

This work is supported by the Fund of Scientific Research−Flanders (FWO), KU Leuven (GOA 11/003), Belgian Federal Science Policy Office (IAP-7/05), and Volkswagen Foundation Project AZ.85101-85103, SENSOR. This research has also received funding from the European Research Council under the European Union's Seventh Framework Programme (FP7/2007-2013)/ERC Grant Agreement No. 340324. S.-L.L. is an FWO Pegasus Marie Curie Fellow.

■ REFERENCES

(1) Moulton, B.; Zaworotko, M. J. *Chem. Rev.* **2001**, *101*, 1629.
(2) Desiraju, G. R. *J. Am. Chem. Soc.* **2013**, *135*, 9952.
(3) Ahn, S.; Matzger, A. J. *J. Am. Chem. Soc.* **2010**, *132*, 11364.
(4) Sirtl, T.; Song, W.; Eder, G.; Neogi, S.; Schmittel, M.; Heckl, W. M.; Lackinger, M. *ACS Nano* **2013**, *7*, 6711.
(5) Zhang, X.; Chen, T.; Chen, Q.; Deng, G.-J.; Fan, Q.-H.; Wan, L.-J. *Chem.—Eur. J.* **2009**, *15*, 9669.
(6) Elemans, H.; Lei, S.; De Feyter, S. *Angew. Chem., Int. Ed.* **2009**, *48*, 7298.
(7) Kim, K.; Plass, K. E.; Matzger, A. J. *Langmuir* **2003**, *19*, 7149.
(8) Ahn, S.; Matzger, A. J. *J. Am. Chem. Soc.* **2012**, *134*, 3208.
(9) Mali, K. S.; Schwab, M. G.; Feng, X.; Müllen, K.; De Feyter, S. *Phys. Chem. Chem. Phys.* **2013**, *15*, 12495.
(10) Gutzler, R.; Sirtl, T.; Dienstmaier, J. R. F.; Mahata, K.; Heckl, W. M.; Schmittel, M.; Lackinger, M. *J. Am. Chem. Soc.* **2010**, *132*, 5084.
(11) Bellec, A.; Arrigoni, C.; Schull, G.; Douillard, L.; Fiorini-Debuisschert, C.; Mathevet, F.; Kreher, D.; Attias, A.-J.; Charra, F. *J. Chem. Phys.* **2011**, *134*, 124702.
(12) Blunt, M. O.; Adisoejoso, J.; Tahara, K.; Katayama, K.; Van der Auweraer, M.; Tobe, Y.; De Feyter, S. *J. Am. Chem. Soc.* **2013**, *135*, 12068.
(13) Yang, Y.; Wang, C. *Curr. Opin. Colloid Int.* **2009**, *14*, 135.
(14) Kampschulte, L.; Lackinger, M.; Maier, A.-K.; Kishore, R. S. K.; Griessl, S.; Schmittel, M.; Heckl, W. M. *J. Phys. Chem. B* **2006**, *110*, 10829.
(15) Lei, S.; Tahara, K.; De Schryver, F. C.; Van der Auweraer, M.; Tobe, Y.; De Feyter, S. *Angew. Chem., Int. Ed.* **2008**, *47*, 2964.
(16) Ciesielski, A.; Szabelski, P. J.; Rżysko, W.; Cadeddu, A.; Cook, T. R.; Stang, P. J.; Samorì, P. J. *Am. Chem. Soc.* **2013**, *135*, 6942.
(17) Lee, S.-L.; Chi, C.-Y. J.; Huang, M.-J.; Chen, C.-h.; Li, C.-W.; Pati, K.; Liu, R.-S. *J. Am. Chem. Soc.* **2008**, *130*, 10454.
(18) Quante, H.; Müllen, K. *Angew. Chem., Int. Ed.* **1995**, *34*, 1323.
(19) Weil, T.; Vosch, T.; Hofkens, J.; Peneva, K.; Müllen, K. *Angew. Chem., Int. Ed.* **2010**, *49*, 9068.
(20) Zan, X.; Feng, S.; Balizan, E.; Lin, Y.; Wang, Q. *ACS Nano* **2013**, *7*, 8385.
(21) Ostwald, W. *Z. Phys. Chem.* **1897**, *22*, 289.
(22) Bhattarai, A.; Mazur, U.; Hipps, K. W. *J. Am. Chem. Soc.* **2014**, *136*, 2142.
(23) Lee, S.-L.; Yuan, Z.; Chen, L.; Mali, K. S.; Müllen, K.; De Feyter, S. *J. Am. Chem. Soc.* **2014**, *136*, 4117.
(24) Schweicher, G.; Paquay, N.; Amato, C.; Resel, R.; Koini, M.; Talvy, S.; Lemaur, V.; Cornil, J.; Geerts, Y.; Gbabode, G. *Cryst. Growth Des.* **2011**, *11*, 3663.
(25) Balandina, T.; Tahara, K.; Sändig, N.; Blunt, M. O.; Adisoejoso, J.; Lei, S.; Zerbetto, F.; Tobe, Y.; De Feyter, S. *ACS Nano* **2012**, *6*, 83.
(26) Lamberti, G. *Chem. Soc. Rev.* **2014**, *43*, 2240.